MDPI

Article

Numerical Simulation Study of Salt Cavern CO$_2$ Storage in Power-to-Gas System

Weizheng Bai [1,2], Jun Lu [3], Jian Wang [3], Xinghui Fu [4], Yaping Fu [3], Yashuai Huang [1,2], Xiao Wang [5] and Xilin Shi [1,2,*]

1   State Key Laboratory of Geomechanics and Geotechnical Engineering, Institute of Rock and Soil Mechanics, Chinese Academy of Sciences, Wuhan 430071, China; weizbai_whrsm@163.com (W.B.)
2   University of Chinese Academy of Sciences, Beijing 100049, China
3   PipeChina Energy Storage Technology Co., Ltd., Shanghai 200122, China
4   Jiangsu Suyan Jingshen Co., Ltd., Huai'an 223200, China
5   State Key Laboratory for Geomechanics and Deep Underground Engineering, School of Mechanics and Civil Engineering, China University of Mining and Technology, Xuzhou 221116, China
*   Correspondence: xlshi@whrsm.ac.cn

Abstract: China's renewable energy sector is experiencing rapid growth, yet its inherent intermittency is creating significant challenges for balancing power supply and demand. Power-to-gas (PtG) technology, which converts surplus electricity into combustible gas, offers a promising solution. Salt caverns, due to their favorable geological properties, are among the best choices for large-scale underground energy storage in PtG systems. CO$_2$ leakage along the interlayer and salt rock–interlayer interfaces is a key constraint on the CO$_2$ tightness of subsurface salt caverns. This paper focuses on the critical issue of tightness within salt cavern CO$_2$ storage, particularly in the Jintan region. A coupled hydro-mechanics mathematical model is developed to investigate CO$_2$ transportation and leakage in bedded salt caverns, with key variables such as permeability range, pore pressure evolution, and permeability changes being analyzed. The results reveal that permeability plays a decisive role in determining the CO$_2$ transportation rate and leakage extent within the salt rock layer. Notably, the CO$_2$ transportation rate and influence range in the mudstone interlayer are significantly larger than those in the salt rock over the same period. However, with prolonged storage time, the CO$_2$ transportation rate and pressure increase in both salt rock and mudstone interlayer exhibit a decreasing trend, eventually stabilizing as the CO$_2$ pressure front reaches the boundary of the simulation domain. Furthermore, elevated operating pressure markedly expands the permeability range and results in higher cumulative leakage. For a specific salt cavern, the CO$_2$ leakage range can reach up to 142 m, and the leakage volume can reach 522.5 tonnes with the increase in operating pressure during 35 years of operation. Therefore, the setting of operational pressure should fully consider the influence of permeability and mechanical strength of the salt rock and mudstone interlayer. These findings provide valuable insights into optimizing the sealing performance of salt cavern CO$_2$ storage systems under varying conditions.

Keywords: renewable energy; salt cavern CO$_2$ storage; permeability; operation pressure; leakage assessment

1. Introduction

Large-scale utilization of renewable energy, such as wind and solar power, is crucial in addressing the global energy crisis and environmental problems. By 2023, China's cumulative grid-connected installed capacity is expected to reach 292 GW for wind power and 6.09 GW for solar power. However, the intermittency and randomness of these energy sources pose increasing challenges to power grid stability and operation scheduling. Moreover, issues such as wind and solar curtailment have constrained the large-scale application of renewable energy generation [1,2].

To overcome these challenges, energy storage systems have emerged as a viable solution, capable of mitigating the volatility of renewable energy generation and promoting its large-scale utilization [3]. Among various storage options, geological energy storage stands out as the most feasible method for large-scale implementation [4]. Salt caverns, in particular, offer an optimal choice for geologic energy storage, boasting advantages such as low permeability [5], excellent mechanical properties [6], damage self-repairing capabilities [7], and large-scale storage capacity [8,9]. Due to their mentioned advantages, salt caverns have been widely used in gas storage [10], compressed air energy storage, hydrogen storage [11], and helium and petroleum storage.

Concurrently, the role of natural gas in energy utilization continues to strengthen, with its recoverable reserves expanding through technological advancements. The increasing interconnection between power systems and natural gas systems has led to growing interest in dual-grid coupling research. A novel salt cavern electro-to-gas system has been proposed (shown in Figure 1), which can integrate renewable energy sources while facilitating limited carbon dioxide sequestration [12]. In this carbon cycle, renewable energy is used to produce hydrogen through water electrolysis, while captured CO_2 from industrial plants participates in methanation and is stored in salt caverns. This method avoids new CO_2 production and emission, presenting an effective carbon capture, utilization, and storage (CCUS) approach. Pilot plants for PtG are currently operational in several countries, including Germany, Switzerland, the USA, Canada, France, Denmark and Japan [3,13,14]. The principal reaction involved in PtG is the Sabatier reaction for water electrolysis and methanation. The type of geological CO_2 storage includes salt caverns, depleted oil and gas reservoirs, basaltic rocks, deep saline aquifers, etc. [15]. According to Table 1, salt caverns are a good option that can be used to store CO_2 permanently in areas where there are no other storage options, like Alberta and Saskatchewan in Canada, salt caverns built offshore in ultra-deep water in Brazil or other places where the salt deposits are high [12].
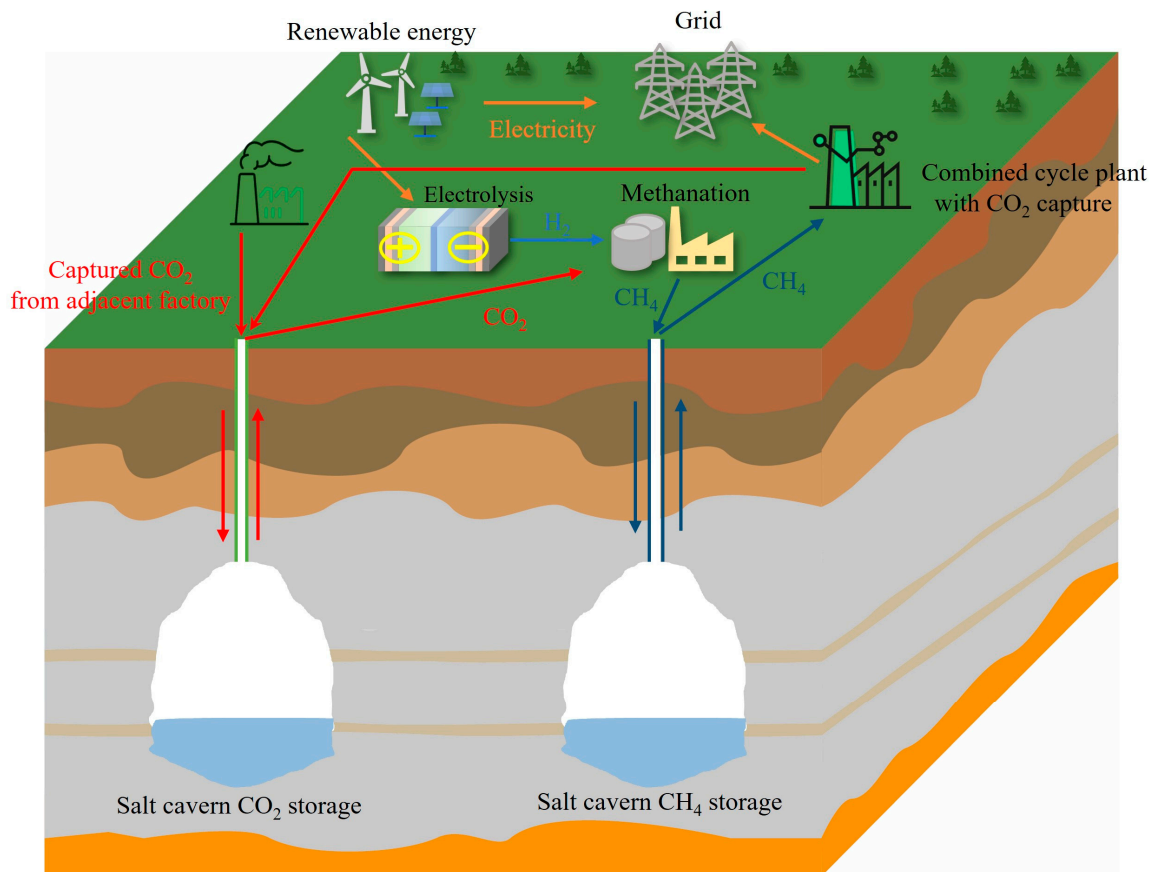
Figure 1. Schematic of underground gas/CO_2 storage in salt caverns [12].

Table 1. The advantages and disadvantages of underground carbon dioxide storage technology.

Type	Advantages	Disadvantages
Depleted reservoirs	Clear volume, better sealing, can be efficiently developed for oil and gas resources in an efficient manner	Small capacity (about 25 billion tonnes of carbon), limited quantity, lack of facilities to transport CO_2
Aquifers	Large capacity (25–90 billion tonnes of carbon) and wide distribution	Uncertain and uncontrollable sealing, complex and uncertain geological features, lack of storage infrastructure
Deep unrecoverable coal seams	Close proximity to CO_2 sources such as large power stations, fuel recovery (CH_4) to reduce costs	Destruction of the subsequent potential value of the coal seam, difficulty in defining whether the seam is mineable or not
Basalt sequestration	Widespread basalt distribution, good basalt injection and storage; low risk of leakage	Limited storage capacity, complex geological environment and difficulty in identifying suitable storage bodies
Salt caverns	The permeability of salt rock is small, and the sealing is good; the damage self-healing is good, and the risk of gas leakage is small; the underground engineering is relatively simple, and the technology is mature. Good economy of building reservoir, relatively low cost.	Stronger creep, larger volume contraction in long-term operation; high-pressure oxygen corrosion under the action of chlorine ions; small injection and extraction pressure interval; relatively small distribution of salt rock layer and restricted site selection.

Salt caverns in China present unique challenges for gas storage due to their predominantly layered formations, characterized by numerous interlayers, thin rock layers, and high impurity content [16,17]. These characteristics necessitate careful study of the confinement properties of bedded salt cavern gas storage reservoirs. Previous research has primarily employed numerical simulation methods to investigate gas seepage characteristics and leakage mechanisms in salt rock caverns [18,19]. Most mathematical models of gas leakage in salt caverns have assumed single-phase gas flow in salt rock and interlayers, considering factors such as periodic pressure fluctuations [20], gas slip effects, and seepage at salt layer–interlayer interfaces [21]. The injection of CO_2 causes an increase in pore pressure in the injected area, and according to the effective stress principle, if the total stress is held constant, the effective stress of the rock mass will decrease, leading to an increase in pore volume, but favoring CO_2 transportation and diffusion, and then affecting the stress and pore pressure fields in the wider area. In general, CO_2 injection has little effect on the total vertical stress of the rock mass, which is approximately equal to the gravity of the overlying rock mass, but the total shear stress changes significantly; both shear and vertical effective stresses are reduced by the increase in pore pressure, with the vertical effective stress decreasing more significantly. From a mechanical point of view, the above pattern of total and effective stresses is due to the fact that the top of the model is free ground, which allows the rock mass to expand freely in the vertical direction, while the lateral displacement constraints on either side of the model usually limit the expansion of the rock mass in the horizontal direction. Therefore, it is necessary to consider the effect of CO_2 in salt cavern reservoirs under the effect of hydro-mechanics coupling. However, most of the current studies focus on the pore pressure of salt cavern reservoirs, and there are fewer studies on the change in porosity and permeability, which need to be further investigated. However, there remains a significant gap in understanding the leakage behavior of salt caverns with weak interlayers, particularly for CO_2 storage under hydro-mechanics coupling effects. This knowledge gap has implications for CO_2 sequestration efficiency and safety, warranting further exploration.

To address this, this study focuses on the salt mine geological conditions and salt cavern morphological characteristics in the Jintan area of Jiangsu Province. This study selected key evaluation indices, including permeability range, pressure, and permeability changes, to investigate the effects of operational pressures on salt cavern sealing and permeability. Building upon these investigations, this paper established a two-dimensional

seepage model for CO_2 storage in salt caverns as part of a power-to-gas system. This model aims to provide valuable insights for evaluating the construction and safe operation of salt cavern CO_2 storage (SCCS) systems, addressing the unique challenges posed by China's bedded salt rock.

2. Physical Modeling of Salt Cavern Storage

2.1. Distribution of Salt Rock Layers

The Jintan Salt Mine, located in the Zhixiqiao Depression of the North Jiangsu Basin, represents a significant salt rock layer with unique geological characteristics. Developed at the end of the Funing Formation deposition, this salt rock layer covers an area of 60.5 km^2 and exhibits a relatively stable planar and vertical distribution [22]. The formation is buried at depths ranging from 1000 to 1300 m, with a thickness varying between 67.8 and 230.95 m. Geologically, the salt rock layer is characterized by a gentle, slightly undulating structure. A notable feature of this formation is the presence of several mudstone interlayers. These interlayers consist of various lithologies, including calcium-containing manganese mudstone, mudstone, and salt mudstone. The thickness of individual interlayers ranges from 0.28 to 4.91 m, contributing to the complex structure of the salt rock layer. This layered composition and the presence of interlayers have significant implications for the utilization of the Jintan salt mine for gas storage or other applications, as they can affect the overall stability and sealing properties of potential caverns.

2.2. Physical Model

To investigate the characteristics of the Jintan salt mine for potential gas storage, a numerical model based on the salt rock layer distribution and cavern shape was developed. A salt rock layer with a top plate depth of 1000 m for our study was selected, reflecting the typical burial depth of the formation. A two-dimensional model was built to simulate the target salt cavern and its surrounding geology by using COMSOL Multiphysics 6.2 software. The use of 2D models to simulate CO_2 storage in salt caverns has some validity. Although the 3D model is able to capture the complex geological conditions and H-M coupling effects more comprehensively, the 2D model can also provide instructive results in some cases. The computational complexity is greatly reduced. This is particularly important when simulation times are long or when multiple conditions are being analyzed in comparison. Two-dimensional models can provide reasonable estimates of CO_2 leakage, permeability changes and pressure distributions in a shorter period of time, and are suitable for assessing sequestration behavior on a large scale. Compared to 3D models, 2D models are more suitable for rapid preliminary design, screening of storage sites or parameter sensitivity analyses. The simulation area is represented by a rectangle measuring 500 m in length and 70 m in width. Within this area, three layers of weak mudstone interlayers, each with a thickness of 3 m, were incorporated to represent the characteristic layered structure of the Jintan salt formation (shown in Figure 2). At the center of the rectangle, a pear-shaped salt cavern with a height of 64 m and a maximum radius of 40 m, mimicking the typical cavern shape in this mine, was modeled. To monitor the behavior of different geological units, two observation points were introduced within the model: one in the salt rock layer and another in the interlayer. A mesh model with 5295 vertices and 9981 triangle elements was obtained by using the powerful meshing function of COMSOL Multiphysics 6.2 software. The mesh is refined for the surrounding rock and the interlayer, and the mesh is gradually coarsened for the salt layer, which is far away from the cave chamber, in order to ensure the accurate calculation of the permeability field near the cave chamber and the overall efficiency of the calculation. This model setup allows us to effectively simulate and analyze the geomechanical and fluid dynamics processes relevant to gas storage in the Jintan Salt Mine, while balancing computational efficiency with geological accuracy. The convergence criteria used in the study were mainly for the residuals of displacement, stress and fluid pressure. During each step of the solution iteration, the residual difference is judged to be converged for that step when it is less than a given threshold. The coupling

between the fluid and the solid is realized in the iteration, and the convergence is judged according to the coupling change of the fluid pressure and solid stress. In order to ensure the stability and accuracy of the simulation results, the varying time step is chosen. In the initial stage of CO_2 sequestration, the time step is small to capture the high gradient change process (0.1 year), and gradually increases to 5 to 10 years as time passes and the system state stabilizes. This setup effectively balances the computational efficiency with the simulation accuracy.

(a) Model boundary conditions (b) Mesh of the surrounding rock
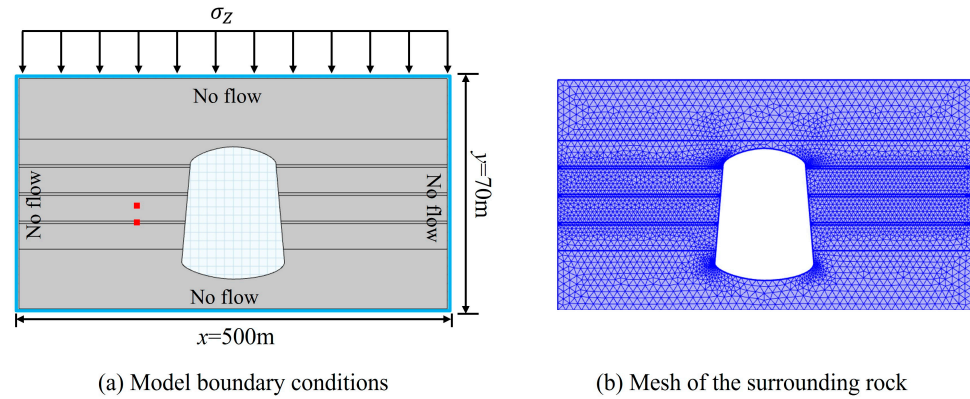
Figure 2. Two-dimensional geological model and mesh grid of the cavern. (**a**) Model boundary conditions, and (**b**) Mesh of the surrounding rock.

2.3. Mesh Independence Test

In general, the greater the density of the mesh, the more precise the resulting calculations will be. However, this also has the effect of considerably increasing the time required for the simulation. In order to enhance the calculation speed while simultaneously ensuring the precision of the simulation results, it is essential to conduct a verification of mesh independence. In the grid division, the primary choices for the largest grid size were $N_{1max} = 0.95$ m, $N_{2max} = 0.85$ m, $N_{3max} = 0.81$ m, and $N_{4max} = 0.61$ m, representing four distinct grid densities. The total numbers of grids were $N_1 = 5142$, $N_2 = 7564$, $N_3 = 9981$, and $N_4 = 14,485$, which were applied in a 12 MPa stratum pressure environment. The objective of the simulation is to ascertain the correlation between the average leakage size in the cavern and the operating pressure of 8 MPa. Figure 3 illustrates the impact of varying grid numbers on the fundamental CO_2 seepage within the salt cavern.
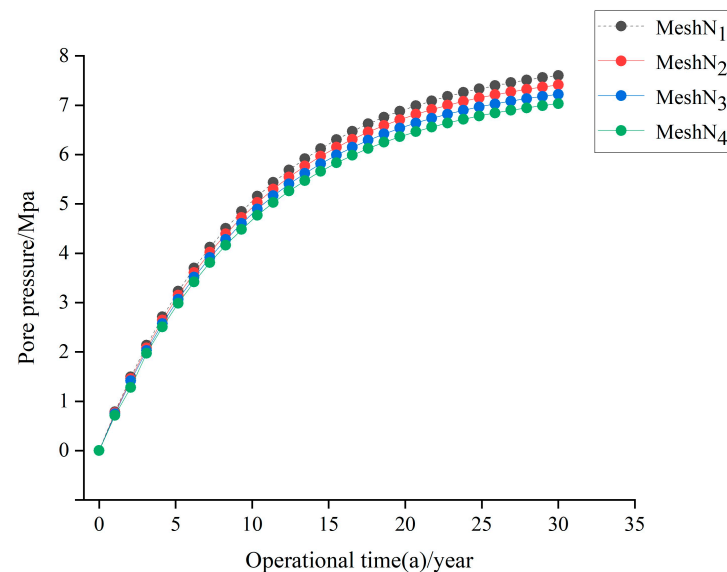
Figure 3. Mesh independence analysis.

As illustrated in the figure, the seepage of CO_2 obtained under four grid densities exhibits a largely consistent trend. When the grid number is N_4, the temperature value is more similar to that of grid number N_1. Additionally, the grid number N_4 demonstrates a more rapid computation speed. This can be applied in the simulation of natural gas injection and extraction processes to satisfy the requirements of grid independence division.

3. Mathematical Modeling

3.1. Model Assumptions

To comprehensively understand the hydro-mechanics (H-M) coupling process during CO_2 storage in salt caverns, a system of partial differential equations was developed. Given the extreme complexity of hydro-mechanics coupling, several simplifying assumptions were necessary to make the numerical calculations feasible while maintaining the model's validity. These assumptions allow us to focus on the most critical aspects of the system while reducing computational complexity. The mathematical model is based on the following key assumptions:

1. Geological structures: Although heterogeneous at the microscopic level, their internal structure is more homogeneous at the large scale and their mechanical and permeability behavior at the macroscopic level can be approximated as isotropic. This simplification can significantly reduce the complexity of the model while having less impact on the actual simulation.

    (a) The salt rock and mudstone interlayers are treated as isotropic, homogeneous, continuous porous media.
    (b) Deformations in these media are assumed to be infinitesimal. This facilitates the calculation process and guarantees that the model can be solved with respect to the hydro-mechanics coupling relationship.

2. Fluid dynamics: The effect of inertial forces can be neglected due to the low fluid seepage velocity. Also, the volumetric forces of CO_2 are relatively small, especially during the sequestration process, and gravity effects have a limited impact on the overall flow of the fluid. These simplifications allow the model to focus on the key influences on hydro-mechanics coupling.

    (a) CO_2 flow in the salt cavern reservoir is modeled as a saturated single-phase flow, adhering to Darcy's law.
    (b) The inertial forces of fluid seepage and rock deformation, as well as the volume force of the fluid, are neglected.

3. Thermal considerations: In salt caverns, temperature changes are typically slow and limited in magnitude, much smaller than the effects of pressure changes. The simplification of ignoring thermal effects allows the model to focus on pressure-dominated coupling effects, as these are the dominant factors in such environments. In addition, the model does not need to take into account complex heat transfer processes and can concentrate on simulating mechanical and fluid processes.

    (a) Temperature effects on fluid density, dynamic viscosity, and heat transfer parameters of both rock and fluid are not considered.
    (b) The solid and fluid phases are assumed to be in constant thermal equilibrium.
    (c) Temperature influences on CO_2 transportation and the deformation of salt rock and mudstone interlayer are disregarded.

3.2. Governing Equations

3.2.1. Elasto-Plasticity Constitutive Equations for Salt Rock and Mudstone Interlayers

Assuming that the pores of the salt rock and mudstone interlayer are filled with gas, the elastic-plastic constitutive relation considering gas pressure is as follows [23]:

$$\Delta\sigma_{ij} = C_{ij}^e(\Delta\varepsilon_t - \Delta\varepsilon_p) - \delta_{ij}\Delta p_g \tag{1}$$

where σ_{ij} is the tensor component of the stress; C_{ij}^e is the initial elastic stiffness matrix of the salt rock and mud interlayer; ε_t is the total strain of the salt rock and mud interlayer; ε_p is the plastic strain of the salt rock and mud interlayer; δ_{ij} is Kronecker notation; p_g is the CO_2 pressure of the salt rock or mud interlayer.

The stress-displacement equation can be expressed as

$$\varepsilon_{ij} = \frac{1}{2}\left(u_{i,j} + u_{j.i}\right) \tag{2}$$

where ε_{ij} is the component of the strain tensor, and u_i is the component of displacement. Since the inertial forces are neglected, the equilibrium equation can be expressed as

$$\sigma_{ij,j} + f_i = 0 \tag{3}$$

where σ_{ij} is the tensor component of the stress, and f_i is the volume force component.

3.2.2. Fundamental Differential Equations for CO_2 Transportation in Salt Rock and Mudstone Interlayers

This equation is a mathematical expression describing the law of transportation of CO_2 in rock. The equation for CO_2 mass conservation in salt rock layers or mudstone interlayers, taking into account Darcy's law, diffusion, and Klinkenberg's effect, is given as follows [24]:

$$\frac{\partial m}{\partial t} + \nabla \cdot (\rho_w q_w) = Q_s \tag{4}$$

where ρ_w is the density of CO_2, kg/s; q_w is Darcy velocity vector, Q_s is sources and sinks of fluids, and m is the mass of CO_2 per unit volume of rock, which is expressed as $m = \rho_w\phi$, where ϕ represents the porosity.

Assuming that gravity effects are small and can be neglected, Darcy's law can be expressed as follows [25]:

$$q_w = -\frac{k}{u}\nabla p \tag{5}$$

where u is the hydrodynamic viscosity, and k is permeability.

The transportation control equations can be obtained by joining Equations (4) and (5):

$$\frac{\partial \rho_w \phi}{\partial t} - \nabla \cdot \left(\frac{k}{u}\rho_w\nabla p\right) = Q_s \tag{6}$$

3.3. Porosity and Permeability Equation

In the mechanical parameters of porous media, porosity occupies a pivotal position. Classical mechanics of fluids in porous media focus on the study of seepage characteristics of porous media. It is generally believed that the skeleton of porous media does not produce deformation, but this assumption is obviously not in line with reality, because the compression deformation caused by changes in ground stress and salt cavern reservoir fluid pressure will cause the skeleton of the porous media to deform to a certain degree. With the increase in reservoir depth, the ground stress and fluid pressure are changed to different degrees, which causes the porosity change accordingly.

According to the porosity, defined as

$$d\varphi = -(1 - \varphi) \times \frac{dV_S}{V_S} + (1 - \varphi) \times \frac{dV_B}{V_B} \tag{7}$$

It is obtained from Equation (7):

$$\frac{1}{1 - \varphi}d\varphi = -\frac{dV_S}{V_S} + \frac{dV_B}{V_B} \tag{8}$$

where φ is porosity, V_B is rock volume, and V_S is the volume of the rock skeleton.

The strain increment of the rock skeleton is

$$\frac{dV_S}{V_S} = -\frac{1}{K_s}dp \tag{9}$$

where K_s is the bulk modulus of the rock skeleton.

The strain increment of the rock as a whole is

$$\frac{dV_B}{V_B} = d\varepsilon_V \tag{10}$$

where ε_V is the volumetric strain of the rock mass.

Coupling Equations (7) and (9), and integrating can obtain

$$\varphi = 1 - (1 - \varphi)\exp\left[-\frac{1}{K_S}(p - p_0) + (\varepsilon_V - \varepsilon_{V0})\right] \tag{11}$$

3.4. Numerical Simulation Scheme and Key Parameters

Based on the operational lifespan of existing salt cavern gas storage reservoirs, the duration of operation for a salt cavern gas storage reservoir should be no less than 30 years. Therefore, this study investigates the CO_2 leakage patterns in a CO_2 salt cavern gas storage reservoir at storage pressures of 8, 12, and 16 MPa over an operational period of 35 years. The simulation time intervals are set at 5, 15, 25, and 35 years, respectively. Using the original salt rock stratum pressure as the initial condition, the specified storage pressure of the salt rock cavern serves as the internal boundary condition. Given that the maximum radius of the salt rock cavern is significantly smaller than that of the surrounding salt rock layer, the external boundary condition is defined as a constant pressure boundary. The key parameters utilized in the simulation process are presented in Table 2.

Table 2. Key parameters for numerical simulation (data from [26]).

| Parameter	Value
Overlying ground pressure/MPa	23.1
Rock salt initial porosity/%	1.00
Mud interlayer initial porosity/%	6.00
Modulus of elasticity of rock salt/GPa	18
Modulus of elasticity of mud interlayer/GPa	10
Initial permeability of rock salt/10^{-8} μm^2	1
Initial permeability of mud interlayer/10^{-6} μm^2	1
Number of mudstone interlayers	3

4. Analysis of Results

4.1. CO₂ Transportation and Leakage Patterns in Salt Caverns

4.1.1. Permeation Range

Figure 4 shows a contour plot of the pore pressure of CO_2 in the salt cavern at different operating pressures. The permeation of CO_2 through the cavern wall is primarily driven by the pressure gradient. When the pore pressure equals the initial pressure of the formation, the pressure gradient becomes zero, causing gas flow to cease. The distance of gas flow is considered the penetration range. Over time, CO_2 will continue to infiltrate the formation, leading to an increase in the penetration range. Given that the porosity and permeability of the mudstone layer are higher than those of the salt layer (with the permeability of the mudstone layer at 1.0×10^{-18} m^2 and that of the salt layer at 1.0×10^{-20} m^2), Darcy's law indicates that the flow rate of gas between layers is faster than that in salt rock. Therefore, the permeability range of the mudstone layer would be greater. The pressure propagation process can be divided into two phases: the extension of the CO_2 impact range to the modelled boundary (operational time 30 a) is the first phase, and the extension of the CO_2

impact range to the modelled boundary (operational time > 30 a) is the second phase. In the first phase, the CO_2 transport rate is faster, the CO_2 influence area gradually expands, the CO_2 pressure within the influence area increases, and the transport rate and pressure increase gradually decrease with the extension of the sequestration time. In the second phase, the CO_2 pressure has propagated to the simulation boundary, the CO_2 pressure at the simulation boundary is increasing, the CO_2 transport pressure difference decreases, the seepage effect of CO_2 transport decreases, and the contribution of diffusion increases, resulting in a further decrease in the rate of CO_2 transport and pressure increase, and tends to stabilize.
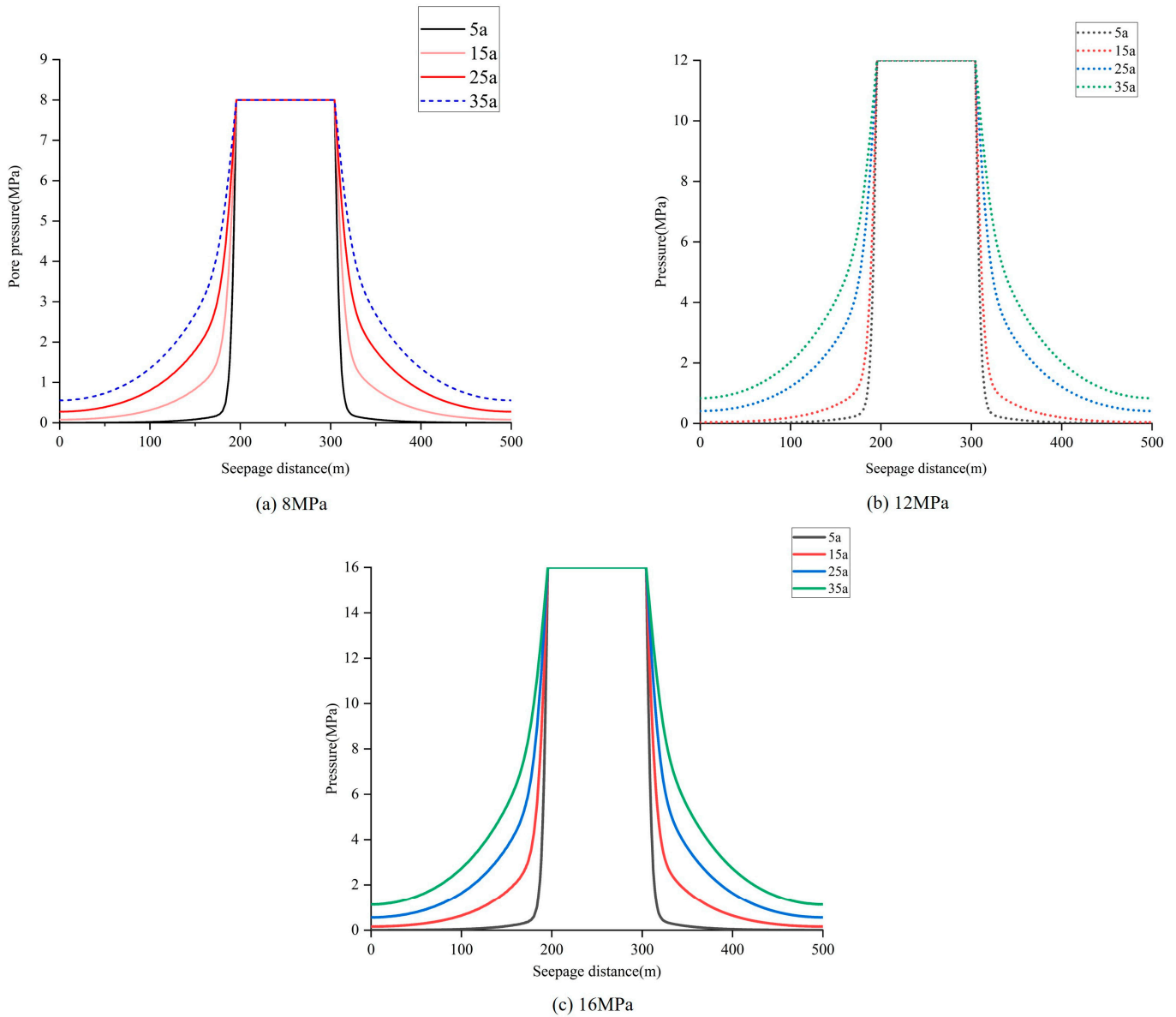

(a) 8MPa
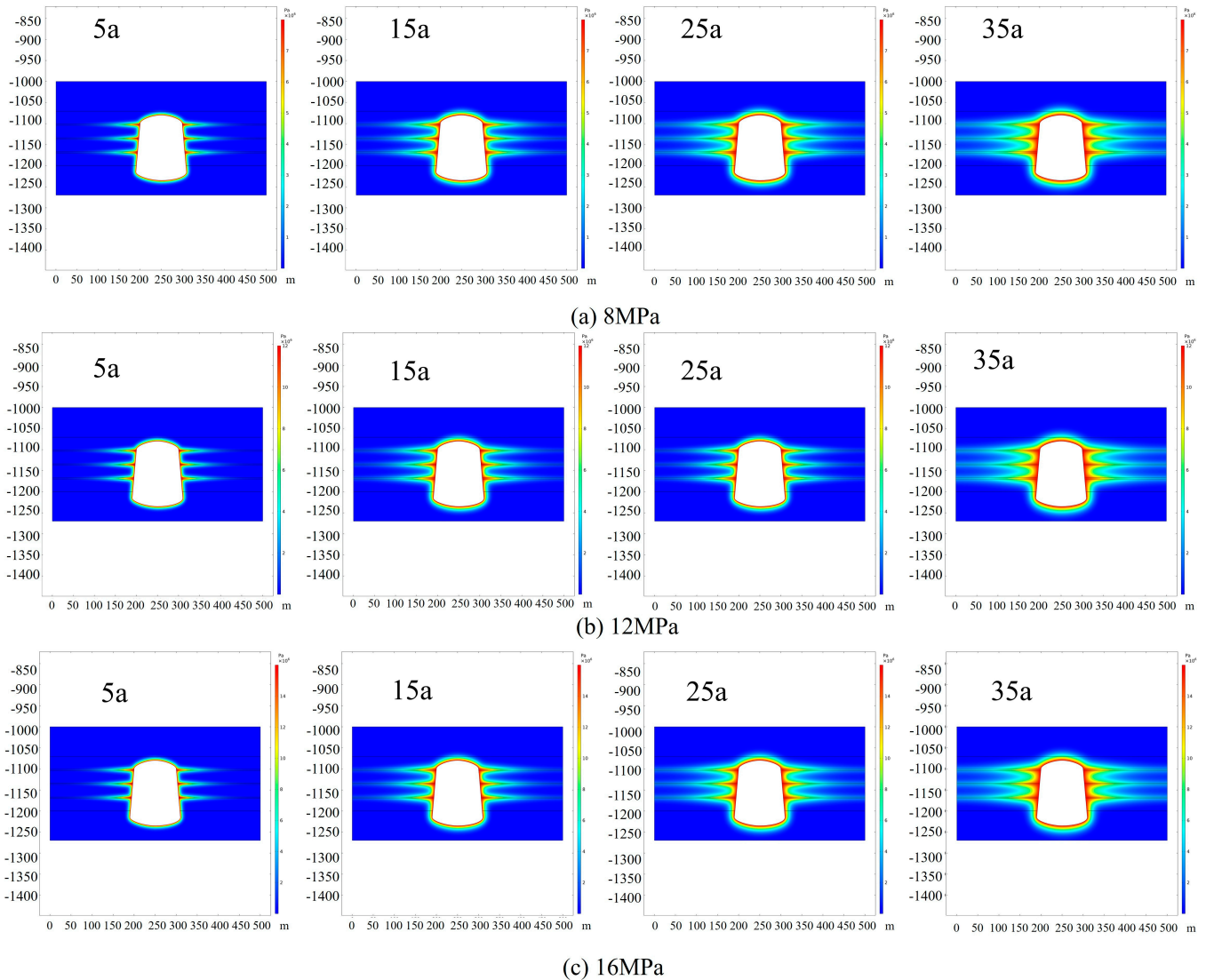
(b) 12MPa

(c) 16MPa

Figure 4. Evolution of the CO_2 seepage range with operational pressure (**a**) 8 MPa, (**b**) 12 MPa, and (**c**) 16 MPa.
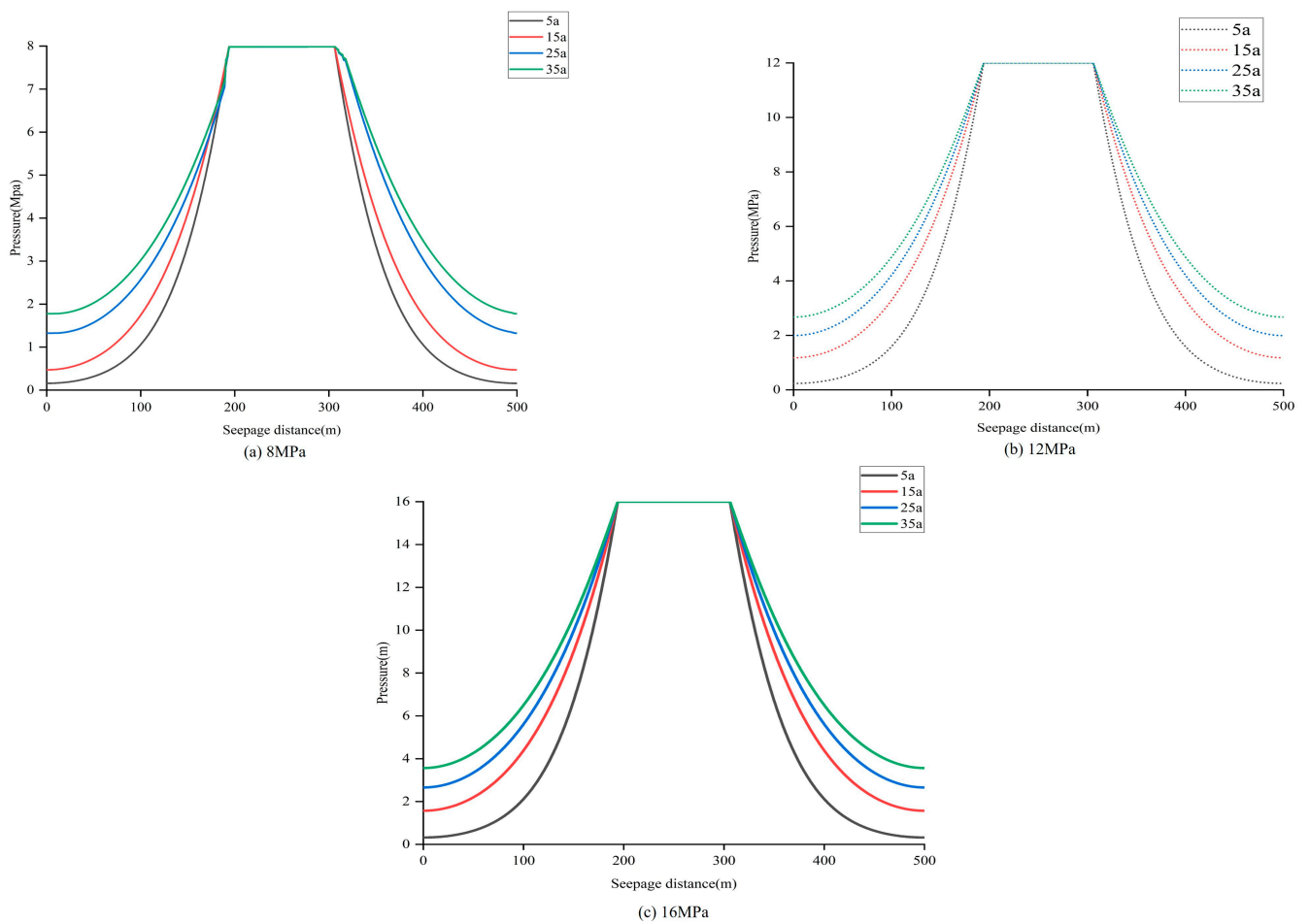
4.1.2. Evolution of CO_2 Pressure at Different Gas Storage Pressures

The storage pressure has no significant effect on the CO_2 transportation rate and influence range within the salt rock layer. Figures 5 and 6 illustrate the relationship between CO_2 pore pressure and the distance. As the permeation distance increases, the pore pressure in the rock layers begins to decrease sharply before gradually leveling off until flow ceases. With an increase in operational time, the pore pressure in the rock layers exhibits similar behavior; however, the pressure drop curve eventually becomes linear, indicating a stable flow rate and steady state of seepage. The pressure drop curve trends

from a rapid decline to a gradual plateau, resembling a concave curve. Compared to the interlayer, the pore pressure drop curve for the salt rock layer is steeper, with a greater slope and shorter permeation range. This is attributed to the lower permeability of salt rock, which results in higher resistance to gas permeation. Figure 7 shows the variation curves of CO_2 seepage range in the interlayer and salt rock, from which it can be seen that the seepage range increases gradually with time and eventually also tends to stabilize; the permeability ranges of the interlayer and the salt rock layer in 30 years are 142.53 m and 31.99 m, respectively, and the permeability range of the interlayer is about 4.45 times as large as that of the salt rock layer.

(a) 8MPa

(b) 12MPa

(c) 16MPa

Figure 5. Evolution characteristics of CO_2 pressure in salt rock at different storage times. (**a**) 8 MPa, (**b**) 12 MPa, (**c**) 16 MPa.

Figure 6. Evolution characteristics of CO_2 pressure in interlayer at different storage times. (**a**) 8 MPa, (**b**) 12 MPa, (**c**) 16 MPa.
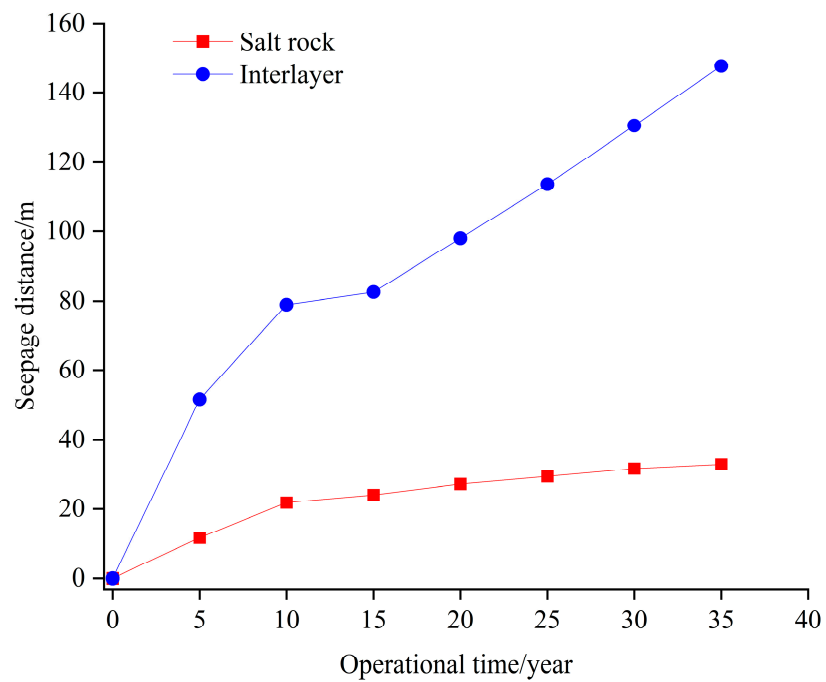
Figure 7. The trend curve of gas seepage range over time.

4.1.3. Leakage Amount

Accurate prediction of CO_2 quality is key to effective gas storage management. For SCCS, cumulative leakage can be used to seal the state of the salt cavern [27,28]. The permeation and diffusion of CO_2 in the surrounding rock may weaken the integrity of adjacent caverns, and a safe distance needs to be set between caverns. During the injection and production period, the cavern pressure undergoes continuous fluctuations. There is a pressure difference between the cavern pressure and pore pressure in the surrounding rock, causing gas to permeate into the surrounding rock or gas to reflux into the cavern. According to Darcy's law, the real-time leakage rate is proportional to the pressure gradient and points in the direction of pressure reduction. It is defined that when CO_2 permeates into the surrounding rock, the CO_2 decreases, and the real-time leakage rate is positive. The CO_2 leakage amount is the integral of the real-time leakage rate over operation time, representing the absolute leakage amount. The leakage ratio is the ratio of the cumulative leakage amount to the total stored mass in the cavern, which is the ratio of the mass of CO_2 permeating in the surrounding rock to the initial stored mass in the cavern [22]:

$$LR = \frac{\int_{t=0}^{t=t_1} m_r dt}{m_t} \tag{12}$$

where m_r is the gas leakage rate, ton/a; m_t is the total stored mass (initial stored mass) in the cavern, in tons. For an SCCS operated for 35 years, the leakage ratio should not exceed 30%, indicating that the cavern meets the sealing requirements. Based on Equation (12), it can be obtained that the cumulative leakage after running 35 years is 522.5 tons, which is 16.55%. This leakage amount meets the requirements.
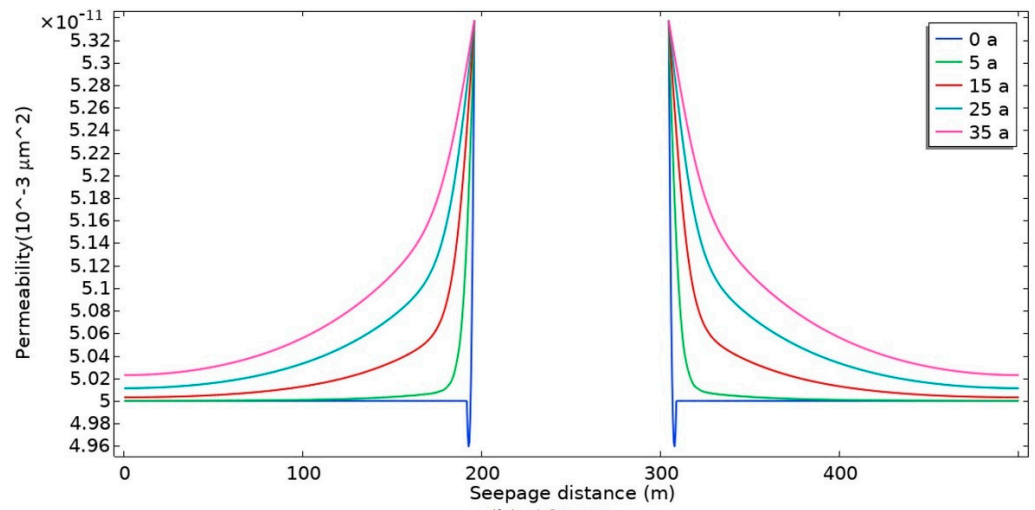
4.2. Patterns of Permeability Evolution

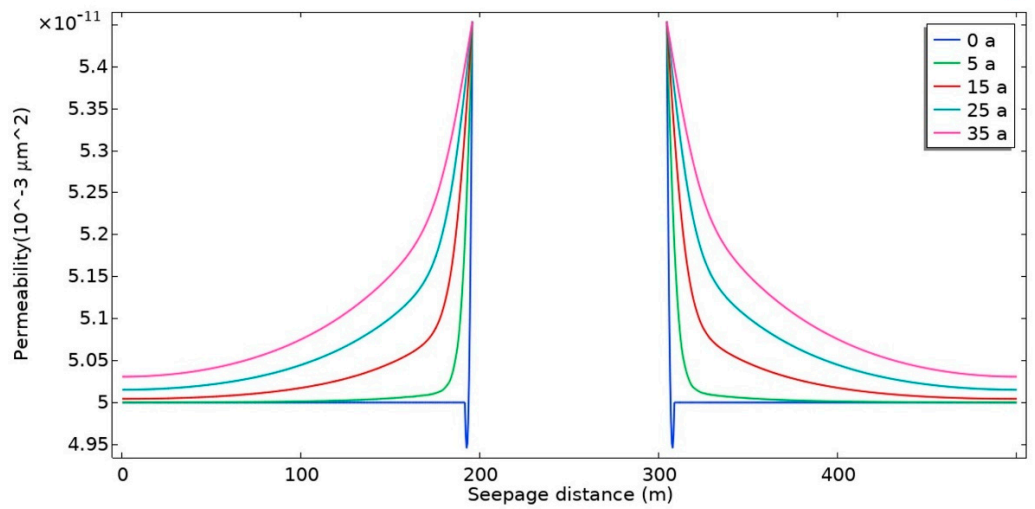4.2.1. Characterization of Permeability Evolution in Salt Rock

As is shown in Figure 1, salt rock permeability is primarily influenced by the pressure of the overlying strata and the CO_2 pressure within the salt rock pores. Under varying CO_2 storage pressures, the permeability of salt rock exhibits a similar pattern of change, which can be categorized into three stages: (1) At the onset of CO_2 sequestration, the range of CO_2 influence in the salt rock is relatively small. Due to the larger overlying formation pressure, the permeability of the salt rock within the simulation range decreases overall, with the rate of reduction increasing as gas storage pressure rises. Notably, in the range of 50–100 m around the cavern, the salt rock permeability reaches its lowest value, due to the combined squeezing effects of gas storage pressure and formation pressure. (2) Prior to the extension of the CO_2 influence range to the simulation boundary (CO_2 sequestration time of 0–25 years), the increase in CO_2 pressure within the salt rock partially counteracts the overlying stratum pressure, resulting in a gradual increase in permeability within the CO_2 influence range. Higher storage pressures correspond to greater increases in permeability; conversely, in areas outside the CO_2 influence range, the permeability gradually decreases and stabilizes at levels observed at the beginning of the sequestration stage (Figure 8). After 5 years of CO_2 sequestration, the permeability of salt rock in the 50–100 m range around the wall of the salt rock cavern significantly recovers. (3) Following the extension of the CO_2 influence range to the boundary of the simulation (sequestration time of 25–35 years), the permeability of the salt rock within the simulation range recovers, with higher storage pressures leading to greater degrees of recovery. These dynamic changes in salt rock permeability result from the combined negative effects of overlying stratum pressure and the positive effects of CO_2 pressure. The reduction in the effective stress on the salt rock due to CO_2 pressure during the leakage and transportation processes is the primary reason for the recovery of salt rock permeability.
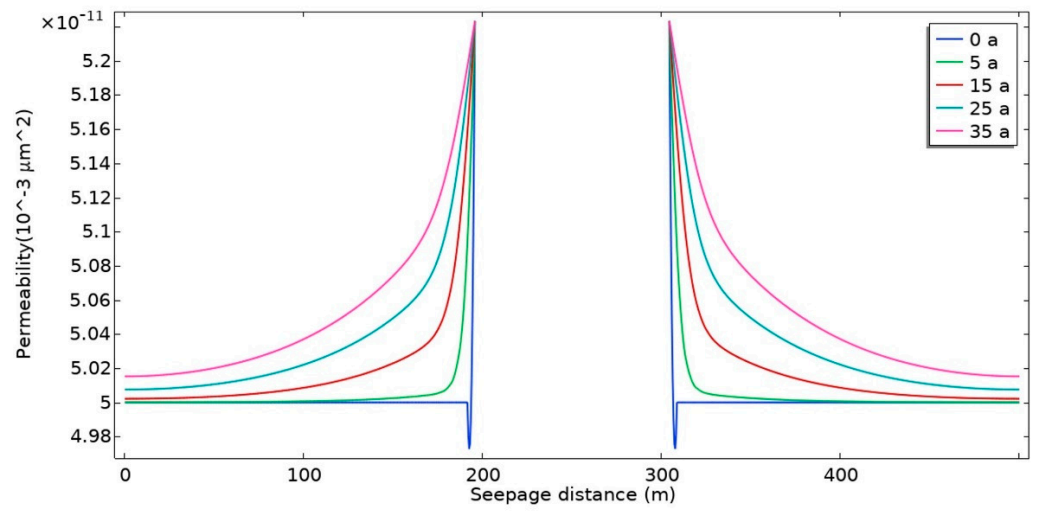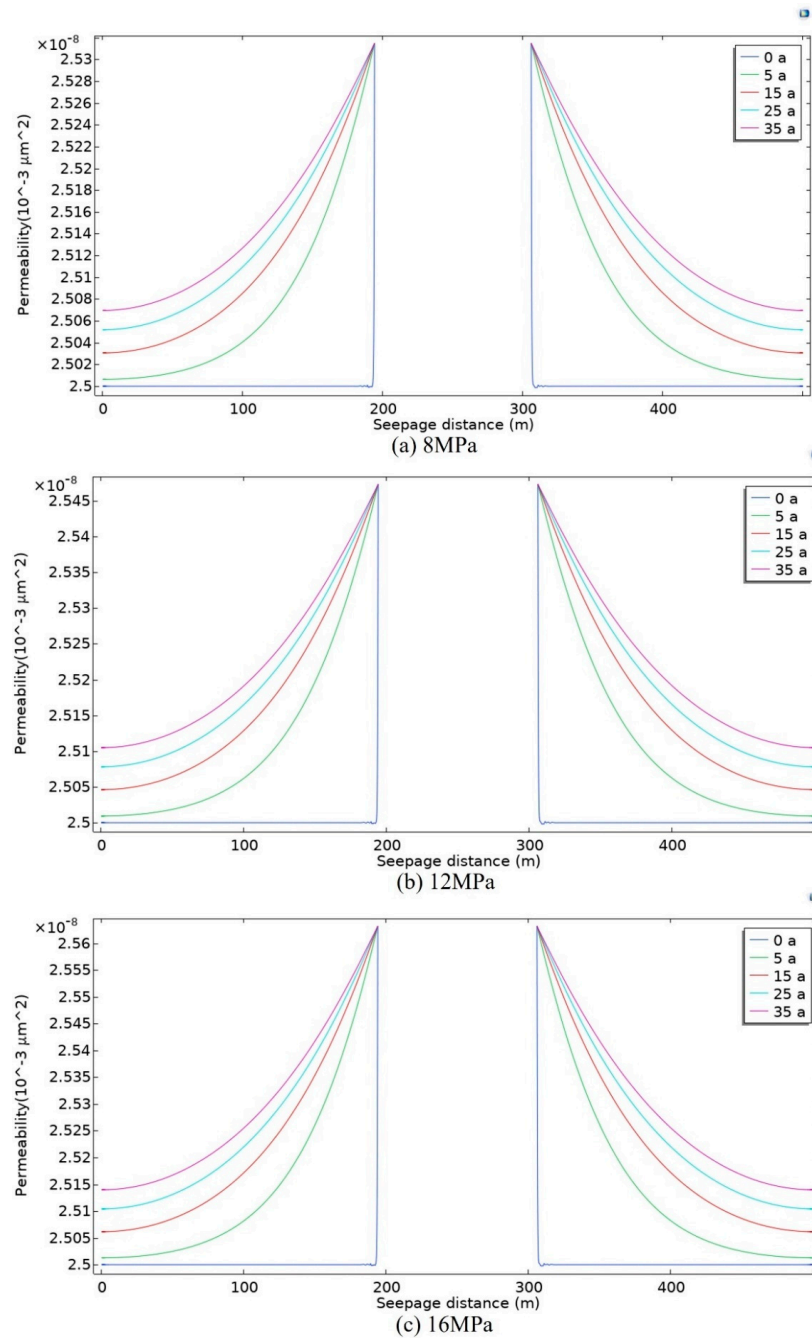
(a) 8MPa

(b) 12MPa

(c) 16MPa

Figure 8. Evolution characteristics of salt rock permeability at different storage times. (**a**) 8 MPa, (**b**) 12 MPa, (**c**) 16 MPa.

4.2.2. Characterization of Permeability Evolution in Interlayer

As is shown in Figure 9, the mudstone interlayer exhibits a pattern of permeability change similar to that of the salt rock. Initially, during CO_2 sequestration (sequestration time is 0 years), the permeability is lower than the initial value due to the pressure from the overlying strata. As sequestration continues, the permeability of the mudstone interlayer within the CO_2 influence range increases, while outside this range, it continuously decreases under the pressure of the overlying strata. The modulus of elasticity of mudstone (10 GPa) is significantly lower than that of salt rock (18 GPa), making it more susceptible to deformation under effective stress. Moreover, the permeability of the mudstone interlayer is relatively high, and the impacts of overburden pressure and CO_2 pressure on its permeability are more pronounced compared to salt rock.

Figure 9. Evolution characteristics of mudstone interlayer permeability at different storage times. (**a**) 8 MPa, (**b**) 12 MPa, (**c**) 16 MPa.

5. Discussion

5.1. Effect of Interlayer on Permeability

The mudstone interlayers play a dominant role in CO_2 migration and leakage compared to salt rock. While salt rock offers a more secure containment with very low permeability, the mudstone interlayers require more careful monitoring and protective measures to prevent leakage and ensure long-term storage security. The effect on permeability relative to salt rock consists of the following three aspects:

(1) Higher permeability of mudstone: Mudstone interlayers typically have a much higher permeability compared to salt rock. This results in faster CO_2 transportation through the interlayers, making them the primary pathways for leakage. While salt rock has extremely low permeability and slows down CO_2 movement, mudstone interlayers allow CO_2 to be transported more freely, which can lead to leakage if not adequately monitored and controlled.

(2) Elasticity differences: The mudstone layer has a lower elastic modulus compared to salt rock, which makes it more susceptible to deformation under pressure. The combined effect of overlying formation pressure and CO_2 injection pressure affects the permeability of mudstone more significantly than salt rock. This means that during CO_2 storage, the permeability of mudstone interlayers can increase more easily due to deformation, further contributing to leakage.

(3) Dynamic permeability changes: The permeability of both salt rock and mudstone changes over time as CO_2 pressure spreads through the storage cavern. Initially, the overlying formation pressure reduces the permeability in both materials. However, as CO_2 pressure increases, the permeability in the mudstone interlayers tends to recover more rapidly than in salt rock, further enhancing the leakage risk along these interlayers.

5.2. Limitations of the Model

In contrast to other studies, the present study pays special attention to the effect of SCCS operational pressure on the recovery of permeability in salt rock and mudstone interlayers. Unlike conventional single-phase seepage models, this study shows that the recovery of mudstone interbedded permeability is faster at higher pressures, leading to potential seepage risks associated with increased sequestration pressures. In contrast, conventional models tend to ignore the permeability recovery effect of pressure increase, whereas this study indicates that pressure should be optimized during operation to balance sequestration stability with the permeability recovery effect to reduce the long-term leakage risk of CO_2. Although the numerical model of CO_2 storage developed in this study can effectively simulate the CO_2 transportation and leakage patterns in bedded salt cavern reservoirs, the results are still limited by several assumptions and simplifications, which may lead to some deviations from the actual situation. The specific limitations are shown below:

① Simplified assumptions of geological conditions:

Isotropic and homogeneous assumptions: The model assumes that the saltstone and mudstone interlayers are isotropic and homogeneous porous media. However, the actual stratigraphy tends to have large heterogeneity, especially in localized areas, where the mechanical properties and permeability of the saltstone and mudstone may show anisotropy. This simplification may ignore the complex fluid transportation paths and local stress concentration phenomena in the actual sequestration process.

② Small deformation assumption:

Small deformation amplitude of salt rock and mudstone is assumed in the model, which is applicable to relatively low pressure and small displacement conditions. In actual gas storage, large deformations or long-term creep effects may occur with pressure changes and time, which are not accounted for in the model and may lead to an underestimation of the long-time storage behavior.

③ Neglect of thermal effects:

The effects of temperature on CO_2 migration and deformation of salt rocks and mudstones are not considered in this model. However, in real life, temperature variations in the repository may affect the density and viscosity of CO_2 as well as rock mechanical properties. The assumption of ignoring thermal effects simplifies the model calculations, but may lead to an underestimation of CO_2 diffusion rates and permeability changes.

④ Simplification of the 2D model:

Simulation using a 2D model, although effective under conditions of high lateral homogeneity, ignores the complex leakage pathways and stress distributions that a 3D model may reveal. The irregular shape and localized 3D heterogeneity of salt caverns are not adequately captured in 2D models and may lead to an underestimation of local leakage risk.

⑤ Prediction of long-term behavior:

The model assumes predictable changes in mechanical and permeability properties over time during CO_2 sealing; however, real long-term geological processes, such as chemical reactions or long-term creep behavior, may lead to unpredictable changes in the sealing and permeability of the storage reservoir. These long-term effects are not fully incorporated in the modelling and may affect the long-term safety assessment of CO_2 storage.

6. Prospects

The simulation results regarding the transportation and leakage characteristics of CO_2 in salt caverns, as well as the dynamic evolution of permeability in salt rock and associated weak interlayers, demonstrate that the permeability of salt rock is exceptionally low, resulting in a slow transportation rate of CO_2 within this medium. However, it is important to note that the majority of salt caverns in China consist of bedded salt rocks interspersed with several interlayers that exhibit significantly higher permeability than the salt rocks themselves. Additionally, the lower modulus of elasticity of these interlayers renders them more susceptible to the effects of overlying formation pressure and CO_2 pressure on their permeability. Therefore, preventing CO_2 leakage along the mudstone interlayers is critical to achieving long-term safe storage of CO_2 in salt caverns. Based on the findings from this simulation study, engineering recommendations and suggestions are provided concerning the site selection, construction, and operation of salt cavern:

(1) In terms of site selection, it is essential to conduct a thorough exploration of the tectonic features, distribution of salt rock layers, and physical parameters of both salt rock and mudstone interlayers prior to the creation of caverns. The selection of sites for salt cavern gas storage reservoirs should aim to avoid areas or layers where mudstone interlayers are prevalent. If avoidance is not feasible, it is advisable to choose locations characterized by a lower number of mudstone interlayers, reduced permeability, and higher mechanical strength for cavern creation [29,30].

(2) In terms of construction, if the cavern area or layer contains mudstone interlayers, it is crucial to construct the CO_2 salt cavern gas storage reservoir in a manner that adequately protects these interlayers. This may involve implementing suitable cementing and leakage prevention technologies, as well as utilizing technological measures to minimize CO_2 leakage along the mudstone interlayers.

(3) From an operational perspective, it is essential to design and implement a long-term monitoring program that includes the monitoring of pressure, CO_2 concentration, and surface deformation. Regular risk assessments and updates to predictive models should be conducted. Additionally, a dynamic pressure monitoring system should be established, accompanied by a rigorous pressure management strategy. It is imperative that gas storage pressure is maintained below the safety threshold.

7. Conclusions

In this study, comprehensive evaluation indices such as permeability range, permeability volume, and dynamic responses of permeability and porosity were introduced to

analyze and evaluate gas leakage and safety in CO_2 reservoirs within salt cavern storage, utilizing a hydro-mechanics coupling seepage theory model. A two-dimensional geological model was developed to simulate and analyze the effects of varying operating pressures on the CO_2 permeability range and the permeability of both salt rock and interlayers. The following conclusions were drawn:

(1) The CO_2 transportation rate and leakage range primarily depend on the permeability of salt rock and mudstone interlayers, which affects the efficacy of CO_2 sequestration within the saltstone caverns. Both the CO_2 transportation rate and pressure increases in the salt rock and mudstone interlayer decrease with prolonged sequestration time; specifically, when the CO_2 storage period exceeds 25 years, the CO_2 pressure reaches the simulation boundary, leading to a gradual stabilization of both the CO_2 transportation rate and pressure increase. Due to differences in permeability, the CO_2 transportation rate and influence range in the mudstone interlayer are significantly greater than those in the salt rock over the same storage period, allowing CO_2 to migrate from the mudstone interlayer to the salt rock, thereby increasing the CO_2 pressure in the salt rock. While the gas storage pressure has no significant effect on the CO_2 transportation rate and influence range within the salt rock layer, the rate of increase in CO_2 pressure in the salt rock layer tends to slow down as gas storage pressure rises. Salt rock and mudstone interlayers have similar permeability dynamics, and the change in permeability of both is a result of the negative effect of the overlying stratum pressure and the positive effect of the CO2 pressure in the salt rock, and is affected by the mechanical properties of the saltstone and mudstone interlayers as well as the pressure of SCCS.

(2) An increase in operating pressure significantly increases the range of penetration and cumulative leakage. For example, at a set average operating pressure of 8 MPa (pin = 8~16 MPa), the leakage ranges of CO_2 in the intercalated layer and the salt-rock layer within 30 years can reach 112.53 m and 31.99 m, respectively, with the permeation range in the intercalated layer being about 3.52 times that in the salt-rock layer. However, none of them exceeds the limit value agreed in the specification. Therefore, the salt rock reservoir can satisfy the requirement of tightness, and basically no leakage accident will occur. Meanwhile, in 35 years of operation, the cumulative leakage reached 522.5 tonnes.

(3) In the process of hydro-mechanics coupling analysis, the formation's permeability and porosity change in response to deformation. The results of the hydro-mechanics coupling calculations indicate that the porosity and permeability of the strata near the cavern wall increase significantly, with a higher rate of permeability growth. The extent of this effect is related to the distance of the formation from the salt cavern; the closer the formation is to the cavern, the greater the influence on permeability parameters. For instance, the permeability of the salt rock layer at the cavern wall is 1.45 times the initial value, representing a 45% increase, while the permeability of the mudstone layer at the cavern wall is 1.06 times the initial value, indicating only a 6% increase. This suggests that the mechanical parameters of the mudstone interlayer are superior to those of the salt rock, and that the permeability of the mudstone interlayer is less affected by disturbances from geostress and operating pressure. Since the porosity and permeability of the formation, when considering hydro-mechanics coupling, are increased, the calculated gas permeability range will be larger than that derived without considering hydro-mechanics coupling. This approach enhances accuracy and safety in the analysis of gas storage confinement.

(4) In terms of future research, in order to investigate the safety of long-term SCCS, it is necessary to establish a long-term creep-permeability coupling model for salt rock, to predict the evolution of the geometry of the salt cavern storage, and to accurately predict the mechanical properties of the mudstone intermediate layer. In terms of numerical modelling, the phase change of CO_2 and its dissolution with brine must be taken into account, and a complete thermal–hydraulic–mechanical–chemical

multi-field coupling model must be established for the temperature change and well response induced by CO_2 injection. These studies will provide a more robust scientific basis for the promotion and application of SCCS technology.

Abbreviations and Nomenclature

PtG	Power to gas
H-M coupling	Hydro-mechanics coupling
CCUS	Carbon capture, utilization, and storage
SCCS	Salt cavern CO_2 storage
σ_{ij}	Tensor component of the stress
C_{ij}^e	Initial elastic stiffness matrix of salt rock and mud interlayer
ε_t	Total strain of salt rock and mud interlayer
ε_p	Plastic strain of salt rock and mud interlayer
δ_{ij}	Kronecker notation
p_g	CO_2 pressure of salt rock or mud interlayer
ε_{ij}	Component of the strain tensor
u_i	The component of displacement
σ_{ij}	Tensor component of the stress
f_i	The volume force component
ρ_w	Density of CO_2, kg/s
q_w	Darcy velocity vectors
Q_s	Sources and sinks of fluids
m	The mass of CO_2 per unit volume of rock
ϕ	Porosity,%
u	Hydrodynamic viscosity
k	Permeability, μm^2
V_B	Rock volume
V_S	Rock skeleton volume
K_s	The bulk modulus of the rock skeleton
ε_V	The volumetric strain of the rock mass

References

1. Gao, R.; Wu, F.; Zou, Q.; Chen, J. Optimal Dispatching of Wind-PV-Mine Pumped Storage Power Station: A Case Study in Lingxin Coal Mine in Ningxia Province, China. *Energy* **2022**, *243*, 123061. [CrossRef]
2. Sadeq, A. *Energy Storage Systems: A Comprehensive Guide*; Qatar Naval Academy: Khasooma, Qatar, 2023; ISBN 9798990783652.
3. Gahleitner, G. Hydrogen from Renewable Electricity: An International Review of Power-to-Gas Pilot Plants for Stationary Applications. *Int. J. Hydrogen Energy* **2013**, *38*, 2039–2061. [CrossRef]
4. Xie, Y.; Wu, X.; Hou, Z.; Li, Z.; Luo, J.; Lüddeke, C.T.; Huang, L.; Wu, L.; Liao, J. Gleaning Insights from German Energy Transition and Large-Scale Underground Energy Storage for China's Carbon Neutrality. *Int. J. Min. Sci. Technol.* **2023**, *33*, 529–553. [CrossRef]

5. Liu, W.; Ding, W.; Fan, J.; Chen, J.; Liu, W.; Jiang, D. Creep Properties and Constitutive Model of Salt Rocks under a Slow Cyclic Loading Path. *J. Energy Storage* **2023**, *72*, 108761. [CrossRef]

6. Han, Y.; Ma, H.; Yang, C.; Li, H.; Yang, J. The Mechanical Behavior of Rock Salt under Different Confining Pressure Unloading Rates during Compressed Air Energy Storage (CAES). *J. Pet. Sci. Eng.* **2021**, *196*, 107676. [CrossRef]

7. Chen, J. Studies on Temperature Effect of Mechanical Properties and Micro Mechanism of Rock Salt. Ph.D. Thesis, Wuhan Institute of Rock and Soil Mechanics, Chinese Academy of Science, Wuhan, China, 2008.

8. Liu, W.; Zhang, Z.; Chen, J.; Jiang, D.; Wu, F.; Fan, J.; Li, Y. Feasibility Evaluation of Large-Scale Underground Hydrogen Storage in Bedded Salt Rocks of China: A Case Study in Jiangsu Province. *Energy* **2020**, *198*, 117348. [CrossRef]

9. Li, H.; Ma, H.; Liu, J.; Zhu, S.; Zhao, K.; Zheng, Z.; Zeng, Z.; Yang, C. Large-Scale CAES in Bedded Rock Salt: A Case Study in Jiangsu Province, China. *Energy* **2023**, *281*, 128271. [CrossRef]

10. Vandeginste, V.; Ji, Y.; Buysschaert, F.; Anoyatis, G. Mineralogy, Microstructures and Geomechanics of Rock Salt for Underground Gas Storage. *Deep Undergr. Sci. Eng.* **2023**, *2*, 129–147. [CrossRef]

11. Huang, L.; Fang, Y.; Hou, Z.; Xie, Y.; Wu, L.; Luo, J.; Wang, Q.; Guo, Y.; Sun, W. A Preliminary Site Selection System for Underground Hydrogen Storage in Salt Caverns and Its Application in Pingdingshan, China. *Deep Undergr. Sci. Eng.* **2024**, *3*, 117–128. [CrossRef]

12. Zhang, X.; Liu, W.; Chen, J.; Jiang, D.; Fan, J.; Daemen, J.J.K.; Qiao, W. Large-Scale CO_2 Disposal/Storage in Bedded Rock Salt Caverns of China: An Evaluation of Safety and Suitability. *Energy* **2022**, *249*, 123727. [CrossRef]

13. Bailera, M.; Lisbona, P.; Romeo, L.M.; Espatolero, S. Power to Gas Projects Review: Lab, Pilot and Demo Plants for Storing Renewable Energy and CO_2. *Renew. Sustain. Energy Rev.* **2017**, *69*, 292–312. [CrossRef]

14. Wulf, C.; Linßen, J.; Zapp, P. Review of Power-to-Gas Projects in Europe. *Energy Procedia* **2018**, *155*, 367–378. [CrossRef]

15. Aminu, M.D.; Nabavi, S.A.; Rochelle, C.A.; Manovic, V. A Review of Developments in Carbon Dioxide Storage. *Appl. Energy* **2017**, *208*, 1389–1419. [CrossRef]

16. Wang, T.; Yang, C.; Shi, X.; Ma, H.; Li, Y.; Yang, Y.; Daemen, J.J.K. Failure Analysis of Thick Interlayer from Leaching of Bedded Salt Caverns. *Int. J. Rock Mech. Min. Sci.* **2015**, *73*, 175–183. [CrossRef]

17. Liu, W.; Li, Y.; Yang, C.; Daemen, J.J.K.; Yang, Y.; Zhang, G. Permeability Characteristics of Mudstone Cap Rock and Interlayers in Bedded Salt Formations and Tightness Assessment for Underground Gas Storage Caverns. *Eng. Geol.* **2015**, *193*, 212–223. [CrossRef]

18. Huang, X.; Xiong, J. Numerical Simulation of Gas Leakage in Bedded Salt Rock Storage Cavern. *Procedia Eng.* **2011**, *12*, 254–259. [CrossRef]

19. Xiong, J.; Huang, X.; Ma, H. Gas Leakage Mechanism in Bedded Salt Rock Storage Cavern Considering Damaged Interface. *Petroleum* **2015**, *1*, 366–372. [CrossRef]

20. Liu, W.; Zhang, Z.; Fan, J.; Jiang, D.; Li, Z.; Chen, J. Research on Gas Leakage and Collapse in the Cavern Roof of Underground Natural Gas Storage in Thinly Bedded Salt Rocks. *J. Energy Storage* **2020**, *31*, 101669. [CrossRef]

21. Li, P.; Li, Y.; Shi, X.; Zhu, S.; Ma, H.; Yang, C. Gas Tightness around Salt Cavern Gas Storage in Bedded Salt Formations. *Renew. Energy* **2024**, *233*, 121191. [CrossRef]

22. Song, Y.; Song, R.; Liu, J. Hydrogen Tightness Evaluation in Bedded Salt Rock Cavern: A Case Study of Jintan, China. *Int. J. Hydrogen Energy* **2023**, *48*, 30489–30506. [CrossRef]

23. Xianjun Tan; Weizhong Chen; Jianping Yang; Chunhe Yang Study of THM-damage coupling model of gas storage in salt rock with interlayer. *Rock Soil Mech.* **2009**, *30*, 3633–3641. (In Chinese) [CrossRef]

24. Cosenza, P.; Ghoreychi, M. Effects of Very Low Permeability on the Long-Term Evolution of a Storage Cavern in Rock Salt. *Int. J. Rock Mech. Min. Sci.* **1999**, *36*, 527–533. [CrossRef]

25. Liu, W.; Muhammad, N.; Chen, J.; Spiers, C.J.; Peach, C.J.; Deyi, J.; Li, Y. Investigation on the Permeability Characteristics of Bedded Salt Rocks and the Tightness of Natural Gas Caverns in Such Formations. *J. Nat. Gas Sci. Eng.* **2016**, *35*, 468–482. [CrossRef]

26. Liu, W.; Dong, Y.; Zhang, Z.; Li, L.; Jiang, D.; Fan, J.; Chen, J.; Zhang, X.; Wan, J.; Li, Z. Optimization of Operating Pressure of Hydrogen Storage Salt Cavern in Bedded Salt Rock with Multi-Interlayers. *Int. J. Hydrogen Energy* **2024**, *58*, 974–986. [CrossRef]

27. Liu, W.; Duan, X.; Li, Q.; Wan, J.; Zhang, X.; Fang, J.; Jiang, D.; Chen, J. Analysis of Pressure Interval/Injection and Production Frequency on Stability of Large-Scale Supercritical CO_2 Storage in Salt Caverns. *J. Clean. Prod.* **2023**, *433*, 139731. [CrossRef]

28. Mwakipunda, G.C.; Mgimba, M.M.; Ngata, M.R.; Yu, L. Recent Advances on Carbon Dioxide Sequestration Potentiality in Salt Caverns: A Review. *Int. J. Greenh. Gas Control* **2024**, *133*, 104109. [CrossRef]

29. Liu, Y.; Li, Y.; Ma, H.; Shi, X.; Zheng, Z.; Dong, Z.; Zhao, K. Detection and Evaluation Technologies for Using Existing Salt Caverns to Build Energy Storage. *Energies* **2022**, *15*, 9144. [CrossRef]

30. Fibbi, G.; Del Soldato, M.; Fanti, R. Review of the Monitoring Applications Involved in the Underground Storage of Natural Gas and CO_2. *Energies* **2023**, *16*, 12. [CrossRef]